# Measurement of the Curvature-Dependent Surface Tension in Nucleating Colloidal Liquids

V. D. Nguyen,[1] F. C. Schoemaker,[1] E. M. Blokhuis,[2] and P. Schall[1]
[1]Van der Waals-Zeeman Institute, University of Amsterdam, Science Park 904, 1098 XH Amsterdam, Netherlands
[2]Leiden Institute of Chemistry, Leiden University, Einsteinweg 55, 2333 CC Leiden, Netherlands

(Received 12 April 2018; published 14 December 2018)

The curvature dependence of the surface tension is central to the nucleation of liquids, but remains difficult to access experimentally and predict theoretically. This curvature dependence arises from the curvature-dependent molecular structure, which, for small nuclei, can deviate significantly from that of the planar liquid interface. Simulations and density functional theory have been used to predict this curvature dependence, however with contradicting results. Here, we provide the first direct measurement of the curvature-dependent surface tension in nucleating colloidal liquids. We employ critical Casimir forces to finely adjust colloidal particle interactions and induce liquid nucleation, and image individual nuclei at the particle scale to measure their curvature-dependent surface tension directly from thermally excited surface distortions. Using continuum models, we elucidate the interplay between nucleus structure, particle pair potential, and surface tension. Our results reveal a 20% lower surface tension for nuclei of critical size compared to bulk liquids, leading to 3 orders of magnitude higher nucleation rates, thus highlighting the importance of surface tension curvature corrections for accurate prediction of nucleation rates.

DOI: 10.1103/PhysRevLett.121.246102

The nucleation of a liquid from its saturated vapor phase provides an archetypical example of nucleation [1,2], governed by the surface tension that sets an energetic barrier for creating the surface surrounding the liquid phase. This surface tension is believed to vary significantly for small nuclei: as the surface becomes curved at the molecular scale, the molecular structure becomes significantly distorted, and this causes the surface tension to deviate from its value of the planar interface [3]. Simulations [4–7] and density functional theory [8–11] have been used to determine the interface tension of these small nuclei, but with controversial results on curvature corrections for the surface tension, thus compromising accurate predictions of nucleation rates.

The nucleation barrier reflects the competition between the energy cost $\Delta G_{\mathrm{surf}}$, for creating the surface between liquid and vapor, and the energy gain $\Delta G_{\mathrm{bulk}}$ from the condensation of particles into the thermodynamically stable liquid phase. The nucleation energy reaches a maximum $\Delta G_c$ at the critical nucleus radius $R_c$; nuclei are only stable and grow if their radius becomes greater than $R_c$. The nucleation energy barrier $\Delta G_c$ thus depends on the surface tension $\gamma$ and chemical potential difference $\Delta\mu$. Since $\gamma$ varies with surface curvature, this alters the nucleation barrier and predicted nucleation rate. However, from simulations and theory no consensus exists about this curvature dependence. Even the sign of change of the surface tension with respect to the flat interface is not agreed on [12]. Experimental measurements based on macroscopic expansion or diffusion can only determine average nucleation rates, leaving the actual curvature-dependent surface tension of individual nuclei inaccessible.

Colloidal particles interacting via critical Casimir forces provide good models for studying liquid nucleation directly at the particle scale [13]. The particles interact via effective attractive pair potentials [14] similar to those of molecules, exhibiting gas-liquid transitions in close analogy to their molecular counterpart [13]. The attractive critical Casimir force arises from the confinement of solvent fluctuations between the particle surfaces in a near-critical solvent [15–18], and owing to its universal temperature dependence allows unique control of the particle interactions. This enables us to drive the colloidal system reversibly through the gas-liquid transition and to investigate the nucleation process directly as a function of the important parameters $\gamma$ and $\Delta\mu$, that together set the energy barrier of nucleation.

Using this colloidal system, we provide the first measurement of the curvature dependence of the surface tension. We image individual liquid nuclei directly at the particle scale, and measure their curvature-dependent surface tension from analyzing thermally induced surface distortions. We find that the surface tension decreases significantly with decreasing nucleus size; for critical nuclei, it drops by about 20% with respect to that of the flat interface, resulting in nucleation rates 3 orders of magnitude larger than predicted by classical nucleation theory. We elucidate the curvature-dependent nucleus structure and test continuum models of surface tensions at small scale. We show that a simple mean-field model allows reasonable prediction of the surface tension based on the particle-scale structure and

 

pair potential. Our results highlight the importance of curvature corrections for accurate nucleation rate predictions in the nanoscale nucleation of liquids.

To study colloidal liquid nucleation, we suspend poly-*n*-isopropyl acrylamide (PNIPAM) particles in a binary solvent mixture of 3-methyl pyridine (3MP) and heavy water [19] with weight fractions of 0.28 and 0.72, respectively, that matches both the refractive index and density of the particles. The refractive index match allows observation of nucleation deep in the bulk of the suspension, while the buoyancy match prevents sedimentation. The particles exhibit attractive critical Casimir interactions below the phase-separation temperature $T_c = 39.5\,°\mathrm{C}$ of the binary solvent. We vary the critical Casimir forces by offsetting the temperature by a small value $\Delta T$ (between 0.5 °C and 0.2 °C) below $T_c$, corresponding to particle interaction energies between $0.2k_BT$ and $1.5k_BT$. At these temperatures, the particles have a constant radius of $r_0 = d/2 = 250$ nm. At $\Delta T = 0.4\,°\mathrm{C}$ and above, they exhibit sufficiently strong attraction for condensation into a liquid phase to occur.

We elucidate the nucleation and growth of the liquid on an intermediate length scale using dynamic light scattering that measures the size of nuclei from their diffusion in the solvent. The correlation time of fluctuations of the scattered intensity is related to the diffusion coefficient via $D = 1/(q^2\tau)$, which is related to the nucleus radius $R$ via the Stokes-Einstein relation $D = k_BT/(6\pi\eta R)$ [20]. Here, $q$ is the scattering vector and $\eta = 1.2$ mPa s the viscosity of the binary solvent [21]. The resulting mean nucleus radius $\langle R\rangle$ as a function of time reveals two stages of growth, as shown in Fig. 1. The first, $\langle R\rangle \propto t^{1/2}$, indicates the growth is limited by the surface, characteristic for nucleation. The

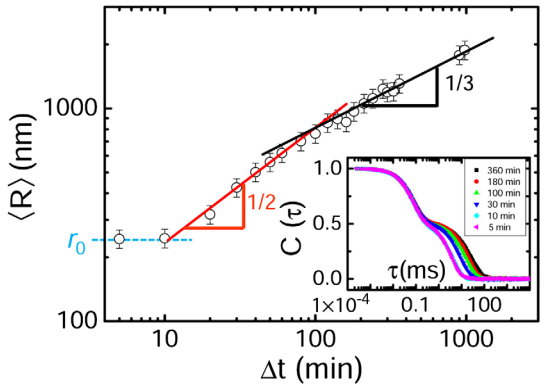


FIG. 1. Light scattering measurement of colloidal liquid nucleation and growth. Mean cluster size as a function of time, determined from the time decay of correlations of the scattered intensity, see inset. The scattered intensity is recorded at a 90° angle with the incident beam after waiting times of $\Delta t = 5$, 10, 30, 100, 180, and 360 min; its autocorrelation $C(\tau)$ (inset) shows double-exponential decays due to solvent fluctuations (at $\tau \sim 10^{-2}$ ms) and colloidal particle clusters (at $\tau \sim 10$ ms) growing in time, shifting the decay to larger $\tau$.

second, $\langle R\rangle \propto t^{1/3}$, indicates the growth is limited by diffusion. This time dependence is similar to the surface- and diffusion-limited growth [22,23] of molecular liquids known as Ostwald ripening [24], highlighting the analogy of the nucleation of colloidal and molecular liquids.

We follow the nucleation process at the particle scale using confocal microscopy to image individual particles in a 66 $\mu$m by 66 $\mu$m by 30 $\mu$m volume, and to determine particle positions with an accuracy of ~0.03 $\mu$m in the horizontal and 0.05 $\mu$m in the vertical direction; the latter is determined from repeated imaging of aggregated particle layers on a cover slip in which thermal motion is suppressed. The direct imaging allows us to visualize the formation and growth of individual nuclei and follow the nucleation process at the particle scale (see movies in Supplemental Material [25]). Initially, small nuclei disappear [Fig. 2(a)], while larger nuclei observed at a later stage are stable and grow [Figs. 2(b) and 2(c)]. Three-dimensional reconstructions show the full structure of typical unstable and stable nuclei in Figs. 2(e)–2(g). The corresponding time-averaged density profiles are plotted in Fig. 2(h). They allow direct measurement of the critical radius $R_c$ of nucleation. The radius of the unstable nucleus is $R \simeq 4r_0$, while that of the stable nucleus is $R \simeq 6r_0$. Thus, $R_c \simeq 5r_0$, which is in good agreement with the crossover observed in dynamic light scattering and simulations of Lennard-Jones liquids yielding critical radii between $4r_0$ and $5r_0$ [4,5] at reduced temperatures corresponding to our colloidal interaction [13].

We also measure the Gibbs free-energy barrier directly from the distribution of nuclei sizes. In thermal equilibrium, the probability $P_N$ for a particle to be in a nucleus of $N$ particles is $P_N \propto \exp(-\Delta G_N/k_BT)$ [4], where $\Delta G_N$ is the Gibbs free energy of the nucleus. Using full three-dimensional reconstructions [Fig. 3(a)], we measure the probability $P_N$ and plot the resultant Gibbs free energy as a function of cluster size in Fig. 3(b). It reaches a maximum of $\Delta G_c \simeq 10k_BT$ at the critical radius $R_c \simeq 5r_0$, in excellent agreement with the direct observation of stable and unstable nuclei. Classical nucleation theory predicts that the Gibbs free energy $\Delta G(R) = 4\pi R^2\gamma - (4\pi/3)R^3\rho\Delta\mu$, where $\gamma$ is the surface tension and $\Delta\mu$ the chemical potential difference with saturation. Using $\rho = 3.3\ \mu\mathrm{m}^{-3}$ determined from Fig. 2(h), we obtain a good fit of the data for $\gamma = 0.33k_BT/d^2$ and $\Delta\mu = 0.52k_BT$ [black solid line in Fig. 3(b)], which are also in good agreement with simulations of Lennard-Jones liquids yielding $\gamma \simeq 0.5k_BT/d^2$ and $\Delta\mu \simeq 0.3k_BT$ at a similar reduced temperature [4,5]. We also explore the effect of varying supersaturation: Performing the experiment at slightly larger $\Delta T$ corresponding to weaker particle attraction, we observe that the nucleation barrier increases and the critical radius grows [red data in Fig. 3(b)]. Fitting with classical nucleation theory gives $\gamma = 0.16k_BT/d^2$ and $\Delta\mu = 0.25k_BT$, both smaller by a factor of ~2, reflecting the lower degree of

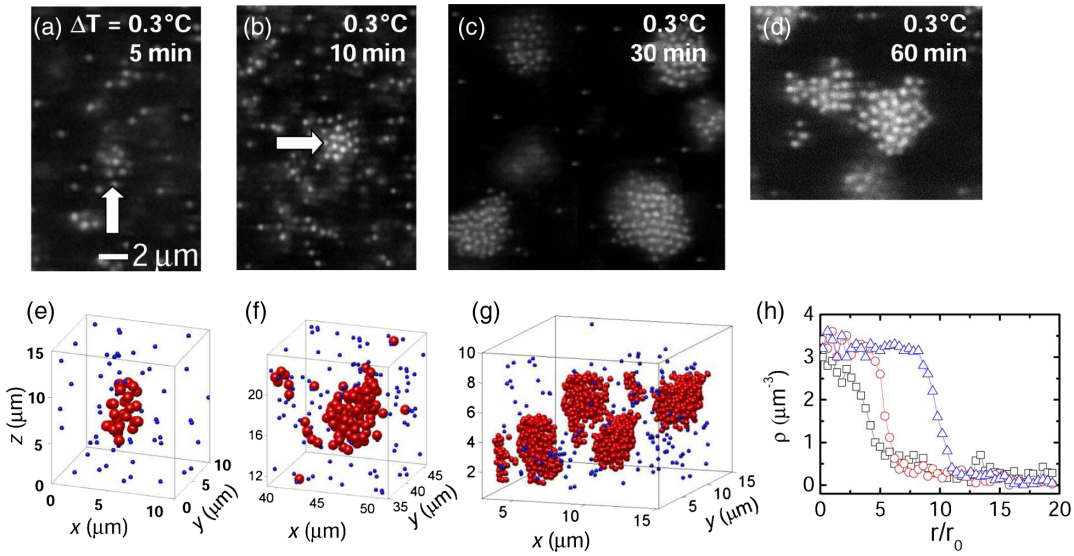


FIG. 2. Colloidal liquid nucleation at the particle scale. (a)–(d) Confocal microscope images of liquid nucleation. (a) Arrow indicates a typical nucleus that disappears after a minute. (b) Arrow indicates a typical nucleus that is stable and grows. (c) Several stable nuclei that have grown to full droplets. (d) Two nuclei merging at later stages, manifesting the well-known Ostwald ripening of molecular liquids. (e)–(g) Reconstructed images of nucleation corresponding to the confocal microscope images (a)–(c). Large red (small blue) spheres indicate particles with more than four (less than or equal to four) nearest neighbors, providing a good representation of liquid and gas particles [4]. Here, nearest neighbors are identified as particles separated by less than $2r_{\min}$, the minimum of the pair correlation function. (h) Time-averaged particle density as a function of distance $r$ from the nucleus center of mass, for the unstable nucleus in (e) (black squares), stable nucleus in (f) (red circles), and a fully grown droplet in (g) (blue triangles). Densities are determined by particle counting. From the images, particle centers are located in three dimensions using recent extensions of the original code by Crocker and Grier [26].

supersaturation due to weaker particle bonds, again in good agreement with simulations [4,5].

We can now address the curvature dependence of $\gamma$ directly. To do so, we focus on individual nuclei and measure their surface tension from analyzing thermally excited surface distortions. Most nuclei are ellipsoidal, exhibiting an excess area $\Delta A$ over the minimum spherical surface area. This excess area is associated with an energy cost $w = \gamma \Delta A$ that, in thermal equilibrium, occurs with probability $P(\Delta A) \propto \exp(-\gamma \Delta A / k_B T)$, allowing us to determine $\gamma$ from the distribution of excess areas $P(\Delta A)$. We use full three-dimensional reconstructions [Fig. 3(a)] to determine, for each nucleus, the best ellipsoidal fit to its surface, and the excess area $\Delta A$ over the spherical shape. The distributions for different sizes of nuclei indeed exhibit a, systematically varying, exponential decay [Fig. 4(a)]; the observed exponential decay of the probability distribution $P(\Delta A)$ with systematically varying slope lends additional credence to this method of determining the surface tension.

The resulting values of the surface tension $\gamma$ obtained from the slope in Fig. 4(a) turn out to increase monotonically with the size of the nucleus [Fig. 4(b)]. To describe the variation of the surface tension and determine curvature corrections, the surface tension results are fitted by a second-order expansion in terms of the inverse radius of the nucleus, $\gamma(R) = \gamma_\infty - 2\delta\gamma_\infty(1/R) - \kappa(1/R)^2$ [27]. Here, $\gamma_\infty$ is the surface tension of the flat interface, $\delta$ the Tolman length that indicates the radius at which the first-order correction becomes of order $\gamma_\infty$ [28], and $\kappa = -2k - \bar{k}$ with $k$ and $\bar{k}$ the bending and Gaussian rigidity, respectively [27]. From simulations and density functional theory, there is no consensus about the sign of the first-order correction, although it is generally believed that its magnitude is significantly less than the molecular diameter [12]. The second-order correction $\kappa$ is believed to be positive and of the order of $1k_BT$, but simulation and density functional theory results are scarce [9–12]. By plotting $\gamma_\infty - \gamma(R)$ normalized to $\gamma_\infty$ as a function of the inverse nucleus radius [Fig. 4(c)], we find $\delta = -0.8d$ and $\kappa = 1.8k_BT$ from the best fit (black line). This value of $\kappa$ lies within simulation values of $1.35k_BT$ and $2k_BT$ [6], respectively, at reduced temperatures higher and lower than in our case (see Supplemental Material [25]).

These direct measurements allow testing continuum models of surface tensions at small scale. The widely used theory of Kirkwood and Buff relates the surface tension to the particle pair potential $U(r)$ and the pair correlation function $g(r)$. Assuming the gas is infinitely dilute and the liquid has a homogeneous density $\rho$ right up to the surface, the surface tension of the planar interface is [29–31]

$$\gamma_{\mathrm{KB}} = \frac{\pi\rho^2}{8}\int_0^\infty dr r^4 U'(r) g(r). \tag{1}$$

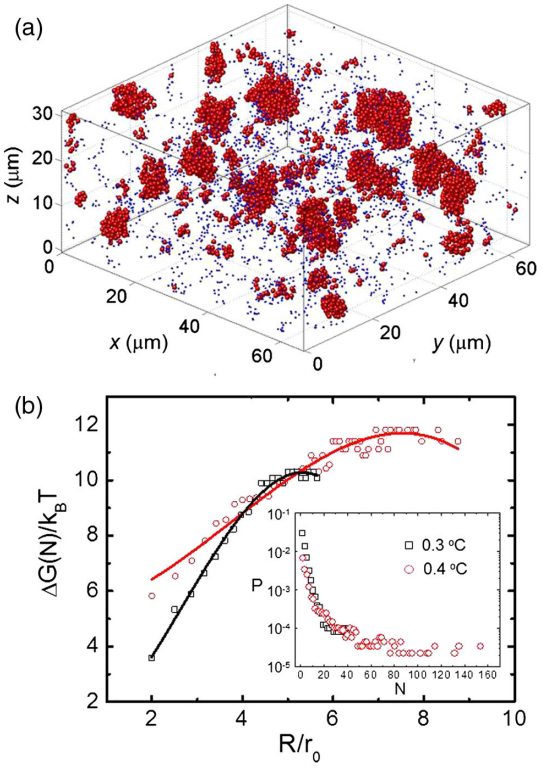


FIG. 3. Gibbs free energy of nucleation. (a) Three-dimensional reconstruction of liquid nuclei coexisting during nucleation equilibrium. (b) Gibbs free energy of nucleation as a function of nucleus radius determined from the relative frequency of cluster sizes (inset), where we have used the particle density $\rho = 3.3\ \mu\text{m}^{-3}$ to convert $N$ to $R$. Black squares show data for $\Delta T = 0.3\,°\text{C}$ corresponding to $T/T_c^{\text{liq}} = 0.72$ [13], with $T_c^{\text{liq}}$ the colloidal liquid critical temperature, and red circles show $\Delta T = 0.4\,°\text{C}$ corresponding to $T/T_c^{\text{liq}} = 0.83$. Solid curves are fits by classical nucleation theory.

We measure $g(r)$ from three-dimensional reconstructions of liquid clusters, and find increasing nearest-neighbor correlations with increasing supersaturation as expected [Fig. 4(d), inset]. We also measure the particle pair potential $U(r)$ directly from the spatial distribution of gas particles [13], and find an attractive minimum, deepening with decreasing $\Delta T$ [Fig. 4(d), main panel], as expected for the growing critical Casimir attraction upon approaching $T_c$. Using these measurements of $g(r)$ and $U(r)$, and taking $\rho = 3.3\ \mu\text{m}^{-3}$, we compute surface tension values by numerical integration. We obtain $\gamma_{\text{KB}} = 0.4 k_B T/d^2$ and $0.2 k_B T/d^2$ at $\Delta T = 0.3°\text{C}$ and $0.4\,°\text{C}$, respectively, in good agreement with the direct measurements in Fig. 4(a). The second-order curvature correction $\kappa$ can likewise be estimated by a mean-field expression similar to Eq. (1) (see Refs. [32,33] and the Supplemental Material [25]). We obtain $\kappa = 1.3 k_B T$, in reasonable agreement with the above direct measurement of $\kappa = 1.8 k_B T$. Our measurement and mean-field estimate of these curvature corrections thus show that both first- and second-order corrections are essential; the resulting $\gamma(R)$ describes the data well down to the critical nucleus size ($N_c \simeq 30$) for which the surface tension has decreased by about 20% of its planar value. Because $\Delta G_c \propto \gamma^3$ [34], this leads to a ~50% lower Gibbs free-energy barrier, resulting in 3 orders of magnitude higher nucleation rates for the nucleation barrier $\Delta G_c \simeq 10 k_B T$ of our system.

Our direct observation of liquid nucleation in colloidal systems, highlighting the importance of curvature corrections of the surface tension, can be translated to molecular liquids. There, the surface tension is typically of the order of 0.1 N/m, 8 orders of magnitude larger than that of our colloidal liquid, reflecting the 8 orders of magnitude higher molecular surface density associated with the 4 orders of magnitude smaller molecular diameter. Consequently, in these molecular systems, activation barriers are typically of the order of $25 k_B T$ [35,36], 3 times higher than that of the colloidal liquid, while the attempt frequency is ~10 orders of magnitude higher. The 20% lower surface tension of critical nuclei then results in nucleation rates ~7 orders of magnitude higher than predicted by classical nucleation theory. Hence, the need for accurate curvature corrections is even more essential for molecular systems than for colloidal systems. Our direct measurement and mean-field estimates of the surface tension for nuclei consisting of a

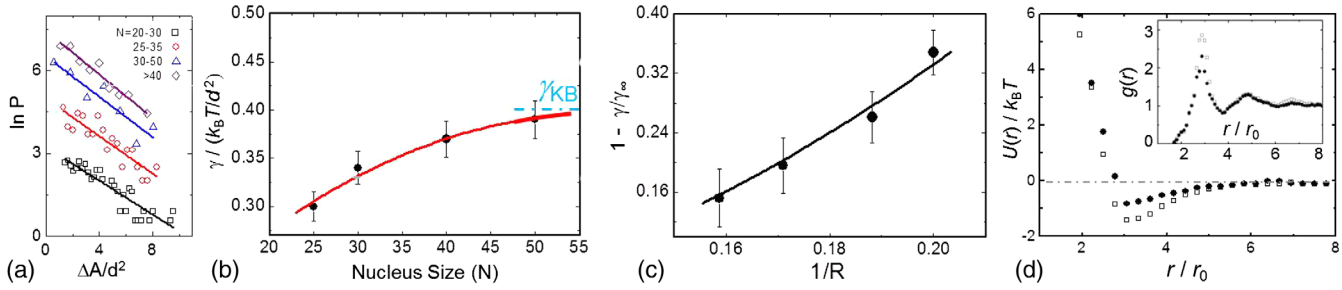


FIG. 4. (a) Distribution of excess areas of ellipsoidal nuclei over the spherical ground state. Symbols distinguish nucleus sizes, see legend. (b) Surface tension of nuclei as a function of size, determined from thermally induced surface shape fluctuations. (c) Same data as in (b), plotted as a function of the inverse nucleus radius. Solid line is a fit up to second order in terms of $(1/R)$. (d) Particle pair potential (main panel) and liquid pair correlation function (inset) for $\Delta T = 0.3\,°\text{C}$ (open symbols) and $\Delta T = 0.4\,°\text{C}$ (closed symbols).

only few tens of particles is of increasing importance as nanoscience pushes material systems to ever smaller dimensions.

P. S. acknowledges support by a Vici grant from the Netherlands Organization for Scientific Research (NWO).


[1] M. Volmer and A. Weber, Z. Phys. Chem. **119**, 227 (1926).
[2] R. Becker and W. Döring, Ann. Phys. (Leipzig) **416**, 719 (1935).
[3] J. W. Gibbs, *The Scientific Papers of J. Willard Gibbs* (Dover, New York, 1961), Vol. 1.
[4] P. R. ten Wolde and D. Frenkel, J. Chem. Phys. **109**, 9901 (1998).
[5] B. J. Block, S. K. Das, M. Oettel, P. Virnau, and K. Binder, J. Chem. Phys. **133**, 154702 (2010).
[6] A. E. van Giessen and E. M. Blokhuis, J. Chem. Phys. **116**, 302 (2002).
[7] J. Merikanto, E. Zapadinsky, H. Vehkamaki, and A. Lauri, Phys. Rev. Lett. **98**, 145702 (2007).
[8] D. W. Oxtoby, in *Fundamentals of Inhomogeneous Fluids*, edited by D. Henderson (Dekker, New York, 1992), and references therein.
[9] A. Malijevsky and G. Jackson, J. Phys. Condens. Matter **24**, 464121 (2012).
[10] E. M. Blokhuis and A. E. van Giessen, J. Phys. Condens. Matter **25**, 225003 (2013).
[11] Ø. Wilhelmsen, D. Bedeaux, and D. Reguera, J. Chem. Phys. **142**, 064706 (2015).
[12] E. M. Blokhuis and J. Kuipers, J. Chem. Phys. **124**, 074701 (2006).
[13] V. D. Nguyen, S. Faber, Z. Hu, G. H. Wegdam, and P. Schall, Nat. Commun. **4**, 1584 (2013).
[14] M. E. Fisher and P.-G. de Gennes, C. R. Acad. Sci. Ser. B **287**, 207 (1978).
[15] M. Fukuto, Y. F. Yano, and P. S. Pershan, Phys. Rev. Lett. **94**, 135702 (2005).
[16] S. Rafai, D. Bonn, and J. Meunier, Physica (Amsterdam) **386**, 31 (2007).
[17] A. Gambassi, A. Maciołek, C. Hertlein, U. Nellen, L. Helden, C. Bechinger, and S. Dietrich, Phys. Rev. E **80**, 061143 (2009).
[18] C. Hertlein, L. Helden, A. Gambassi, S. Dietrich, and C. Bechinger, Nature (London) **451**, 172 (2008).
[19] D. Bonn, J. Otwinowski, S. Sacanna, H. Guo, G. Wegdam, and P. Schall, Phys. Rev. Lett. **103**, 156101 (2009).
[20] C. S. Johnson and D. A. Gabriel, *Laser Light Scattering* (Dover, New York, 1995).
[21] L.-C. Wang, H.-S. Xu, J.-H. Zhao, C. Y. Song, and F.-A. Wang, J. Chem. Thermodyn. **37**, 477 (2005); A. Oleinikova, L. Bulavin, and V. Pipich, Int. J. Thermophys. **20**, 889 (1999).
[22] C. Wagner, Z. Elektrochem. **65**, 581 (1961).
[23] I. M. Lifshitz and V. V. Sloyozov, J. Phys. Chem. Solids **19**, 35 (1961).
[24] W. Ostwald, *Lehrbuch der Allgemeinen Chemie* (Leipzig, Germany, 1896), Vol. 2, Pt. 1.
[25] See Supplemental Material at http://link.aps.org/supplemental/10.1103/PhysRevLett.121.246102 for movies, further experimental details, particle tracking and surface area determination procedure as well as the mean-field expression used to determine the value of the rigidity constant.
[26] See http://tacaswell.github.io/tracking/html/ (Maria Kilfoil's code).
[27] W. Helfrich, Z. Naturforsch. **28C**, 693 (1973).
[28] R. C. Tolman, J. Chem. Phys. **16**, 758 (1948).
[29] J. G. Kirkwood and F. C. Buff, J. Chem. Phys. **17**, 338 (1949).
[30] R. H. Fowler, Proc. R. Soc. A **159**, 229 (1937).
[31] M. V. Berry, R. F. Durrans, and R. Evans, J. Phys. A. Gen. Phys. **5**, 166 (1972).
[32] E. M. Blokhuis and D. Bedeaux, Physica (Amsterdam) **184A**, 42 (1992).
[33] M. Napiórkowski and S. Dietrich, Phys. Rev. E **47**, 1836 (1993).
[34] J. Frenkel, *Kinetic Theory of Liquids* (Oxford University Press, Oxford, 1946).
[35] D. Kashchiev, J. Chem. Phys. **125**, 044505 (2006).
[36] Activation barrier for water at $T = 290$ K and supersaturation of $p/p_e \simeq 7$, where $p_e$ is the equilibrium pressure.